Atmospheric Environment 79 (2013) 334–339

Contents lists available at SciVerse ScienceDirect

Atmospheric Environment

journal homepage: www.elsevier.com/locate/atmosenv

Technical note

Ultrafine particle emissions from desktop 3D printers☆

Brent Stephens [a,*], Parham Azimi [a], Zeineb El Orch [a,b], Tiffanie Ramos [a]

[a] Department of Civil, Architectural and Environmental Engineering, Illinois Institute of Technology, Chicago, IL, USA
[b] National Institute of Applied Sciences (INSA de Lyon), Lyon, France

ARTICLE INFO

Article history:
Received 22 April 2013
Received in revised form
24 June 2013
Accepted 26 June 2013

Keywords:
Indoor aerosols
Three-dimensional printers
Thermoplastic emission
Molten extrusion deposition

ABSTRACT

The development of low-cost desktop versions of three-dimensional (3D) printers has made these devices widely accessible for rapid prototyping and small-scale manufacturing in home and office settings. Many desktop 3D printers rely on heated thermoplastic extrusion and deposition, which is a process that has been shown to have significant aerosol emissions in industrial environments. However, we are not aware of any data on particle emissions from commercially available desktop 3D printers. Therefore, we report on measurements of size-resolved and total ultrafine particle (UFP) concentrations resulting from the operation of two types of commercially available desktop 3D printers inside a commercial office space. We also estimate size-resolved (11.5 nm–116 nm) and total UFP (<100 nm) emission rates and compare them to emission rates from other desktop devices and indoor activities known to emit fine and ultrafine particles. Estimates of emission rates of total UFPs were large, ranging from $\sim 2.0 \times 10^{10}$ # min^{-1} for a 3D printer utilizing a polylactic acid (PLA) feedstock to $\sim 1.9 \times 10^{11}$ # min^{-1} for the same type of 3D printer utilizing a higher temperature acrylonitrile butadiene styrene (ABS) thermoplastic feedstock. Because most of these devices are currently sold as standalone devices without any exhaust ventilation or filtration accessories, results herein suggest caution should be used when operating in inadequately ventilated or unfiltered indoor environments. Additionally, these results suggest that more controlled experiments should be conducted to more fundamentally evaluate particle emissions from a wider arrange of desktop 3D printers.

1. Introduction

Three-dimensional (3D) printers are gaining popularity as rapid prototyping and small scale manufacturing devices. The development of low-cost desktop versions has made this technology widely accessible for use in home and office settings. The majority of commercially available 3D printers utilize an additive manufacturing technique known as molten polymer deposition (MPD), whereby a solid thermoplastic filament is forced through a computer-driven extrusion nozzle (Bumgarner, 2013). The heated nozzle melts the thermoplastic feedstock and deposits streams of extruded plastic in thin layers across a moving baseplate. As the material hardens and the baseplate moves to the next layer, a three-dimensional solid shape is rapidly formed.

Several types of thermoplastics are commonly used in a variety of these commercially available desktop MPD devices. Most desktop 3D printers currently utilize either acrylonitrile butadiene styrene (ABS) or polylactic acid (PLA) as a thermoplastic feedstock (Ragan, 2013). Primary differences between ABS and PLA based printers are feedstock origin and nozzle and baseplate temperatures during operation. PLA is a biodegradable, corn-based plastic that prints at nozzle temperatures of ~180 °C and baseplate temperatures near room temperature. ABS is a stronger thermoplastic that typically prints at ~220 °C nozzle temperatures and ~80 °C baseplate temperatures in most commercially available devices (Weinhoffer, 2012). Other thermoplastic feedstock sources include polyvinyl alcohol (PVA), polycarbonate (PC), and high-density polyethylene (HDPE), although they are not widely used in commercially available devices (Ragan, 2013).

Previous studies of moderately high temperature (e.g., 170–240 °C nozzle temperatures) thermal processing of thermoplastics in large scale industrial extrusion equipment have shown that both gases and particles are emitted during operation (Contos et al., 1995; Unwin et al., 2012). Primary gas-phase products of ABS thermal decomposition at very high temperatures have been shown to include carbon monoxide and hydrogen cyanide, as well

* Corresponding author.
E-mail address: brent@iit.edu (B. Stephens).

1352-2310/$ – see front matter © 2013 The Authors. Published by Elsevier Ltd. All rights reserved.
http://dx.doi.org/10.1016/j.atmosenv.2013.06.050

as a variety of volatile organics (Rutkowski and Levin, 1986). Exposure to thermal decomposition products from ABS has also been shown to have toxic effects in both rats (Zitting and Savolainen, 1980) and mice (Schaper et al., 1994).

Other studies have shown that exposure to fumes from thermal decomposition of other thermoplastics, such as polytetrafluoroethylene (PTFE), is also acutely toxic to mammals, including humans (Oberdörster et al., 2005 and references therein). Moreover, ultrafine particles (UFPs: particles less than 100 nm) may be of particular importance for toxicity of fumes emitted from melting of some thermoplastics. For example, in a previous study of high temperature melting of PTFE at ~480 °C, UFPs with a count median diameter of 18 nm were produced, which were also shown to be highly toxic to rats (Oberdörster et al., 1995). Additional studies revealed that the gas phase of PTFE fumes alone was not acutely toxic (Johnston et al., 2000), which suggests that ultrafine aerosols emitted from thermal degradation of thermoplastic materials may be of concern among emission products generated in these high temperature applications.

Despite the rapid commercial uptake of desktop 3D printers that rely on similar moderate or high temperature thermoplastic melting and extrusion technology, we are not aware of any data on particle emissions from these commercially available devices. Indoor emissions from these devices may be particularly important because they are most often sold as standalone devices without mechanical ventilation or filtration accessories. Therefore, we report on the first measurements of which we are aware of size-resolved and total UFP concentrations resulting from the operation of several models of a single type of commercially available desktop 3D printer utilizing two types of thermoplastic feedstocks and operating inside a small office space. We also estimate individual size-resolved and total UFP emission rates and compare them to other desktop devices and indoor activities known to emit UFPs.

2. Methods

Measurements were conducted in a 45 m^3 furnished and conditioned office space belonging to a company who specializes in 3D printer education, training, and sales for the general public. Nine 3D printers were installed on tables in this particular space; only five adjacent printers were used in this study. Particle number concentrations were measured in the closed room using a TSI NanoScan SMPS Model 3910 logging at 1-min intervals. The SMPS utilizes an isopropanol-based CPC and a radial DMA for size resolution across 13 bins from 10 to 420 nm. It was placed on a table inside the closed room approximately 2 m away from the nearest printer. The door remained closed during the testing procedure except during periods when printers were reset.

We were granted access to the office space only for a limited time and thus relied on an ad hoc experimental design consisting of four distinct operational periods over a period of approximately 2.5 h: (1) background measurements without printers operating for approximately 25 min; (2) two identical 3D printers using PLA thermoplastic feedstocks operating for approximately 20 min to print small plastic figures (followed by a short decay period while the next printing period was setup); (3) the same two PLA-based printers operating simultaneously with three of the same make and model printers operating with higher temperature ABS feedstocks for approximately 20 min to print another set of small plastic figures; and (4) a concentration decay period lasting approximately 40 min. The measured concentration data were used to solve for size-resolved and total UFP emission rates using a combination of methods from the various monitoring periods, as described below.

Increases in particle concentrations during either printer operation period were observed only for particles smaller than the 150 nm bin; therefore we only use data from the first nine particle size bins (11.5 nm–116 nm) in this work. In addition to size-resolved measurements, we also describe total UFPs as the sum of the first eight particle size bins smaller than 100 nm, per existing nomenclature in the field (Oberdörster et al., 2005). The room was assumed to be well-mixed for all periods, which should be reasonable for a small room with several high temperature devices operating over a 2.5 h time period (Baughman et al., 1994; Klepeis, 1999), although we cannot confirm this assumption. However, similar approaches for estimating emission rates from even larger spaces have been used successfully in previous studies (Wallace et al., 2004; Buonanno et al., 2009).

2.1. Period 1: background measurements

Upon arrival to the room the printers had not been operating since the previous day. Particle concentrations were first measured inside the room during this time for a period of ~25 min. Because the resulting concentrations were stable, data from this period was used as the representative steady-state background concentration for each particle size, including total UFPs (i.e., the sum of all particle concentrations less than 100 nm). The background concentration is a function of the fundamental parameters described in Equation (1), although only concentrations were directly measured.

$$C_{i,\mathrm{in,ss,bg}} = \frac{P_i \lambda C_{i,\mathrm{out}}}{L_i} \quad (1)$$

where $C_{i,\mathrm{in,ss,bg}}$ is the mean baseline size-resolved (or total UFP) indoor particle concentration (# cm^{-3}); $C_{i,\mathrm{out}}$ is the size-resolved outdoor particle concentration (# cm^{-3}, not measured in this study); L_i is the size-resolved total loss rate in the room due to the combined effects of air exchange with outside the room, deposition to surfaces, and removal by any operating HVAC system and filter (min^{-1}); P_i is the room penetration factor (dimensionless, not measured); and λ is the air exchange rate in the room (# min^{-1}, not measured). Because of the short access window for the field measurements and limited instrument availability, we were not able to measure the air exchange rate in the office space. However, the total loss rate L_i was estimated from the decay period in this study according to a procedure outlined in the description of Period 4. Total loss rates are then used for estimating emission rates in both Periods 2 and 3. This same procedure has been used successfully in other previous studies of indoor UFP emissions from a variety of devices and appliances (e.g., Wallace et al., 2004; Buonanno et al., 2009).

2.2. Period 2: two PLA printers operating

During Period 2, two 3D printers were operated simultaneously to print sample plastic products. Printer operation continued until the objects were fully printed, which took approximately 20 min. These identical make and model printers utilized a polylactic acid (PLA) feedstock and operated at an extruder temperature of 200 °C and baseplate temperature of 18 °C. One printer assembled a small plastic frog (shown in Fig. 1) and the other assembled a plastic chain link.

UFP concentrations measured during Period 2 were shown to reach approximately steady state before the print jobs were complete (see Fig. 2). Therefore, individual emission rates were estimated using steady-state indoor concentrations ($C_{i,\mathrm{in,ss,2PLA}}$) as shown in Equation (2). Emission rates were assumed to be the same for each PLA printer because they were the same make and model, although we were not able to test the validity of this assumption.

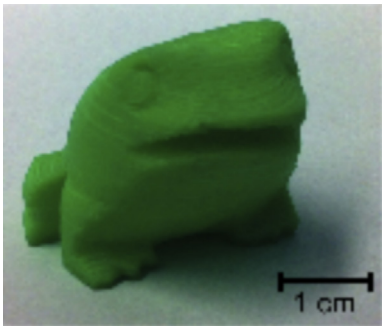

Fig. 1. Example of a three-dimensionally printed frog in this study.

$$C_{i,\mathrm{in,ss,2PLA}} = C_{i,\mathrm{in,ss,bg}} + \frac{2(E_{i,\mathrm{PLA}}/V)}{L_i} \quad (2)$$

where $E_{i,\mathrm{PLA}}$ is the individual size-resolved (or total) UFP emission rate from each of the two PLA printers (# min^{-1}) and V is the volume of the room (cm^3). The mean and standard deviation of the background concentrations from Period 1 were used in conjunction with steady-state data from Period 2 and estimates of L_i from Period 4 to solve for $E_{i,\mathrm{PLA}}$. The procedure was performed using data from each of the nine particle size bins (11.5–116 nm), as well as for the total UFP number concentrations (the sum of all eight UFP bins). Uncertainty in $E_{i,\mathrm{PLA}}$ was estimated as the relative standard deviations from the means for both $C_{i,\mathrm{in,ss,bg}}$ and $C_{i,\mathrm{in,ss,2PLA}}$ added in quadrature with the relative uncertainty in L_i. Period 2 ended when the 3D printers finished printing the models; subsequently there was a short decay period while we prepared additional printers for Period 3 tasks.

2.3. Period 3: two PLA printers and three ABS printers operating

During Period 3, the same two printers from Period 2 utilizing PLA feedstocks were operated again along with three additional printers of the same make and model. However, the three additional printers utilized an ABS feedstock and operated at higher extruder and baseplate temperatures of 220 °C and 118 °C, respectively. Each printer assembled another small plastic frog, with the exception of one of the PLA printers that again assembled a small chain link. Because of the time-varying nature of the data measured during this period, emission rates were estimated using the analytical solution to a dynamic mass balance on the space, as shown in Equation (3).

$$C_{i,\mathrm{in}}(t) = C_{i,\mathrm{in},t=0}e^{-L_i t} + \left[C_{i,\mathrm{in,ss,bg}} + \frac{2(E_{i,\mathrm{PLA}}/V) + 3(E_{i,\mathrm{ABS}}/V)}{L_i}\right] \times \left(1 - e^{-L_i t}\right) \quad (3)$$

A two-parameter nonlinear least squares regression (Stata Version 11) was performed to estimate the size-resolved (and total) UFP emission rates from the combination of all five printers during this period, where $E_{i,\mathrm{total}} = 2E_{i,\mathrm{PLA}}/V + 3E_{i,\mathrm{ABS}}/V$. Both the initial concentration ($C_{i,\mathrm{in},t=0}$) and the total emission rates ($E_{i,\mathrm{total}}$) were treated as unknowns for each particle size (and total UFPs) in the regression analysis. The same values of L_i from Period 4 decay data (which were also used in Period 2) were used in conjunction with mean values of $C_{i,\mathrm{in,ss,bg}}$ from Period 1. Uncertainty in emission rates was estimated as the relative standard error of the regression coefficients for both $E_{i,\mathrm{total}}$ and L_i added in quadrature with the relative standard deviation in $C_{i,\mathrm{in,ss,bg}}$ from Period 1. Size-resolved UFP emission rates for the two PLA printers ($E_{i,\mathrm{PLA}}$) were assumed to be the same as in Period 2 and size-resolved UFP emission rates for each of the three ABS printers ($E_{i,\mathrm{ABS}}$) were also assumed to be equal. As a check on our emission rate estimates, we also estimated size-resolved and total UFP emission rates assuming there were no losses during this brief period of high emissions (where $E_{i,\mathrm{total}} = \Delta C_i V/\Delta t$). This served to provide a reasonable lower bound of emission rates for the printers. This procedure for solving for emission rates neglects any particle coagulation or growth by condensation, which may introduce some additional uncertainty in our estimates of size-resolved emission rates. However, emission rates of total UFPs based on this approach are not affected by coagulation or condensation growth, as these mechanisms only impact individual bins within the total UFP range. Other recent studies have also used a similar methodology neglecting coagulation or condensation, as source strengths are often large enough to overwhelm other impacts within a short period of testing (e.g., Wallace et al., 2004; Afshari et al., 2005; He et al., 2007).

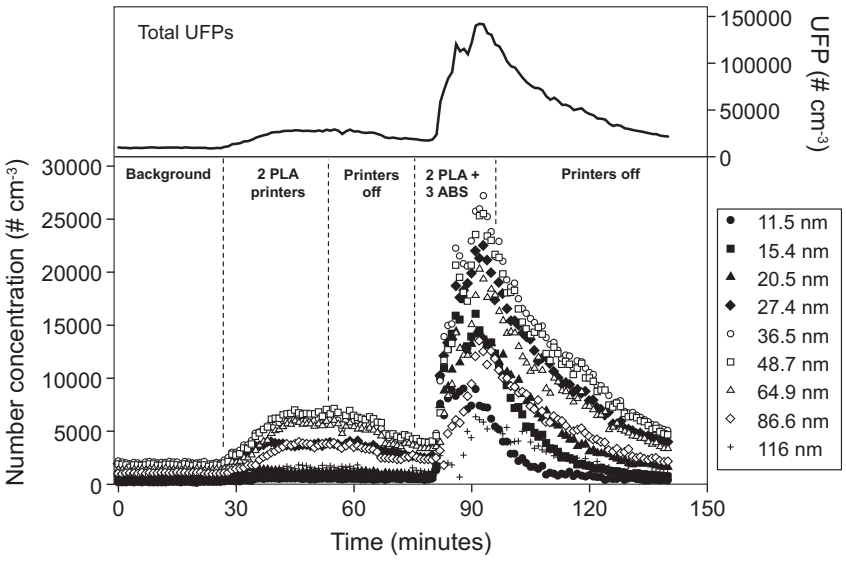

Fig. 2. Size-resolved and total (<100 nm) ultrafine particle (UFP) concentrations measured in the office space during the sampling campaign.

2.4. Period 4: printers off (decay)

Finally, during Period 4, all printers were turned off and indoor concentrations decayed back toward normal background levels. Total loss rates (L_i) were estimated for each particle size and for total UFPs using the time-varying data that fit a straight line on a log-linear plot, as shown in Equation (4).

$$\ln\left(\frac{C_{i,\mathrm{in}}(t) - C_{i,\ \mathrm{in,\ ss\ bg}}}{C_{i,\ \mathrm{in}}(t\ =\ 0) - C_{i,\ \mathrm{in\ ss\ bg}}}\right) - L_i t \tag{4}$$

Estimating loss rates in this manner provides lumped loss rates that account for the combined effects of air exchange, deposition to indoor surfaces, and removal by any HVAC filtration. Unfortunately due to both equipment and access limitations, relative contributions of each of these were not directly measured. However, previous studies have shown this lumped approach to be valid for estimating emission rates (Wallace et al., 2004; Buonanno et al., 2009). Total particle loss rates were assumed to be constant during the relatively short field-testing period of 2.5 h for use in solving for emission rates from the previous periods.

3. Results

Fig. 2 shows resulting time-resolved UFP concentrations measured in the office space throughout the sampling campaign. The bottom portion shows size-resolved number concentrations for the 11.5 nm–116 nm particle size bins (as previously mentioned, no elevations in particle concentrations were observed in particle bins larger than 116 nm and thus are not shown for graphical clarity). The top portion of Fig. 2 also shows total UFP concentrations summed across the first 8 particle size bins smaller than 100 nm.

The operation of the two printers utilizing PLA as a feedstock increased concentrations primarily for particles larger than 20 nm. Indoor concentrations during PLA printer operation also reached approximately steady-state conditions for a period of ~15 min. Subsequently, the operation of the two PLA printers in conjunction with three of the same make and model printers (albeit utilizing a higher temperature ABS feedstock) resulted in substantial increases in all UFP sizes. Table 1 summarizes mean (±s.d.) size-resolved and total UFP concentrations measured during both background (Period 1) and steady-state operation of two PLA-based printers (Period 2), along with peak concentrations from the operation of all five 3D printers (Period 3). Only peak concentrations are shown for each particle size for Period 3 measurements because steady-state conditions were not achieved before the printers finished their print jobs. Table 1 also summarizes loss rates and associated uncertainty estimated from Period 4 data. Regression coefficients showed good correlation between measured and modeled concentrations during the decay period for most particle sizes (except for the smallest and largest size bins).

Mean size-resolved particle concentrations during the operation of the two printers utilizing PLA feedstock were a factor of ~1–4 times higher than during background periods, depending on particle size. Total UFP concentrations were almost three times higher (~27,800 cm^{-3} vs. ~9700 cm^{-3}). The largest increases were observed in the 36–86 nm size ranges. During operation of the same two PLA printers combined with three additional printers utilizing ABS feedstocks, size-resolved particle concentrations rapidly elevated to as high as 9–56 times background and 3.6–31 times that with only two PLA-based printers operating, depending on particle size. Peak total UFP concentrations with all five printers operating (~142,200 cm^{-3}) were five times higher than with only two PLA-based printers operating and nearly 15 times higher than background conditions.

Lumped loss rates estimated from all of the Period 4 decay data ranged from ~2.5 h^{-1} to ~5.6 h^{-1}. Total UFP loss rates were approximately 3 h^{-1}. The largest uncertainty in loss rates was associated with the largest and smallest particle size bins, likely due to relatively low peak concentrations from which decay occurred. Although the relative contributions of air exchange, deposition to surfaces, and control by any HVAC filtration are not known, they are not necessary to solve for emission rates herein (Wallace et al., 2004; Buonanno et al., 2009).

Fig. 3 shows size-resolved and total UFP emission rates and associated uncertainty for individual 3D printers estimated from the measured concentration data following the methodology described in Section 2. The higher temperature ABS-based printers had total UFP emission rates nearly an order of magnitude higher than the lower temperature PLA-based printers ($1.8–2.0 \times 10^{11}$ # min^{-1} compared to $1.9–2.0 \times 10^{10}$ # min^{-1}). Peak emission rates from the PLA-based printers occurred in the 48–65 nm size range while peak emission rates from the higher temperature ABS-based printers occurred in a smaller size range (~15–49 nm). Table 2 describes the same central estimates of UFP emission rates from Fig. 3 along with ranges of uncertainty estimated for each size bin. Additionally, minimum estimates of emission rates made by ignoring particle losses were 30–51% lower than our central estimates; for example, the minimum estimate for the total UFP emission rate from a single ABS printer was 9.7×10^{10} # min^{-1} compared to 1.9×10^{11} # min^{-1} for our best estimate. Therefore, even if there is additional uncertainty in our estimates of emission rates, the ABS printers still have a total UFP emission rate on the order of 10^{11} # min^{-1}.

Several recent studies have also reported size-resolved and/or total UFP emission rates from a variety of other consumer devices, appliances, and activities such as laser printers, candles, cigarettes, irons, radiators, and cooking on gas and electric stoves (e.g., Dennekamp, 2001; Wallace et al., 2004, 2008; Afshari et al., 2005; Buonanno et al., 2009; He et al., 2010). Unfortunately, it is not straightforward to compare our results directly to results from many of these studies because they have varied in both their minimum and maximum measured particle sizes, as well as in their definition of UFPs. However, Buonanno et al. (2009) reported total UFP emission rates over the same size range as ours measured during various cooking activities. For comparison, our estimate of the total UFP emission rate for a single PLA-based 3D printer ($1.9–2.0 \times 10^{10}$ # min^{-1}) was similar to that reported during cooking with an electric frying pan ($1.1–2.7 \times 10^{10}$ # min^{-1}). The same 3D printer utilizing a higher temperature ABS feedstock had an emission rate estimate ($1.8–2.0 \times 10^{11}$ # min^{-1}) similar to that reported during grilling food on gas or electric stoves at low power (1.2–

Table 1
Summary statistics for each test period.

Particle size	Period 1	Period 2	Period 3	Period 4	
	$C_{i,\mathrm{ss,in,bg}}$ (# cm^{-3})	$C_{i,\mathrm{ss,in,2PLA}}$ (# cm^{-3})	$C_{i,\mathrm{in,2PLA\ +\ 3ABS}}$ (# cm^{-3})	L_i (h^{-1})	R^2
	Mean (s.d.)	Mean (s.d.)	Peak		
11.5 nm	158 (25)	495 (33)	8977	4.01 ± 0.20	0.91
15.4 nm	544 (27)	557 (33)	17,438	5.65 ± 0.08	0.99
20.5 nm	975 (25)	1085 (63)	14,356	4.19 ± 0.06	0.99
27.4 nm	1779 (64)	3712 (99)	22,475	2.89 ± 0.05	0.99
36.5 nm	2025 (76)	5976 (164)	27,185	2.58 ± 0.05	0.98
48.7 nm	1793 (76)	6671 (229)	25,473	2.54 ± 0.06	0.98
64.9 nm	1372 (66)	5649 (218)	20,265	2.54 ± 0.06	0.98
86.6 nm	1038 (45)	3695 (161)	13,479	3.09 ± 0.09	0.97
116 nm	695 (58)	1575 (137)	142,211	4.42 ± 0.35	0.80
UFP	9684 (248)	27,838 (658)	6345	2.97 ± 0.04	0.99

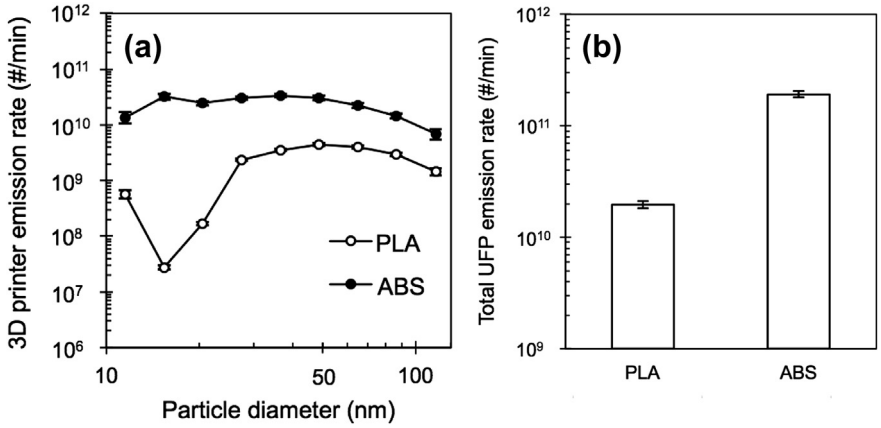

Fig. 3. Individual UFP emission rates from 3D printers utilizing two types of thermoplastic feedstocks in this study: (a) size-resolved emission rates (11.5–116 nm) and (b) total UFP (<100 nm) emission rates.

2.9×10^{11} # min^{-1}), but approximately an order of magnitude lower than gas or electric stoves operating at high power ($1.2–3.4 \times 10^{12}$ # min^{-1}). Regardless, the desktop 3D printers measured herein can all be classified as "high emitters" with UFP emission rates greater than 10^{10} particles per min, according to criteria set forth in He et al. (2007).

4. Discussion

UFPs are particularly relevant from a health perspective because they deposit efficiently in both the pulmonary and alveolar regions of the lung (Hinds, 1999; Chalupa et al., 2004), as well as in head airways. Deposition in head airways can also lead to translocation to the brain via the olfactory nerve (Oberdörster et al., 2004). The high surface areas associated with UFPs also lead to high concentrations of other adsorbed or condensed compounds (Delfino et al., 2005; Sioutas et al., 2005). Several recent epidemiological studies have shown that elevated UFP number concentrations are associated with adverse health effects, including total and cardiorespiratory mortality (Stölzel et al., 2007), hospital admissions for stroke (Andersen et al., 2010), and asthma symptoms (Peters et al., 1997; Penttinen et al., 2001; Von Klot et al., 2002). Therefore, results herein suggest that caution should be used when operating these 3D printing instruments inside unvented or unfiltered indoor environments due to their large emissions of UFPs.

Table 2
Estimates of emission rates from individual 3D printers utilizing different thermoplastic feedstocks.

Particle size bin	UFP emission rates per printer (# min^{-1})			
	PLA (Period 2)		ABS (Period 3)	
	Central estimate	Range	Central estimate	Range
11.5 nm	5.8×10^8	$[4.7–6.8] \times 10^8$	1.4×10^{10}	$[1.1–1.7] \times 10^{10}$
15.4 nm	2.8×10^7	$[2.6–3.0] \times 10^7$	3.2×10^{10}	$[2.8–3.6] \times 10^{10}$
20.5 nm	1.7×10^8	$[1.6–1.8] \times 10^8$	2.5×10^{10}	$[2.2–2.7] \times 10^{10}$
27.4 nm	2.4×10^9	$[2.2–2.5] \times 10^9$	3.0×10^{10}	$[2.8–3.3] \times 10^{10}$
36.5 nm	3.6×10^9	$[3.4–3.7] \times 10^9$	3.4×10^{10}	$[3.2–3.7] \times 10^{10}$
48.7 nm	4.5×10^9	$[4.2–4.7] \times 10^9$	3.1×10^{10}	$[2.8–3.3] \times 10^{10}$
64.9 nm	4.0×10^9	$[3.8–4.3] \times 10^9$	2.2×10^{10}	$[2.0–2.4] \times 10^{10}$
86.6 nm	3.0×10^9	$[2.8–3.2] \times 10^9$	1.5×10^{10}	$[1.3–1.6] \times 10^{10}$
116 nm	1.5×10^9	$[1.2–1.7] \times 10^9$	6.9×10^9	$[5.4–8.5] \times 10^9$
Total UFPs (<100 nm)	2.0×10^{10}	$[1.9–2.0] \times 10^{10}$	1.9×10^{11}	$[1.8–2.0] \times 10^{11}$

One important limitation to this study is that we have no information about the chemical constituents of the UFPs emitted from either type of 3D printer, although condensation of synthetic organic vapors from the thermoplastic feedstocks are likely a large contributor (Morawska et al., 2009). In addition to large differences in emission rates observed between PLA- and ABS-based 3D printers, there may also be differences in toxicity because of differences in chemical composition. As mentioned, thermal decomposition products from ABS have been shown to have toxic effects (Zitting and Savolainen, 1980; Schaper et al., 1994); however, PLA is known for its biocompatibility and PLA nanoparticles are widely used in drug delivery (Anderson and Shive, 1997; Hans and Lowman, 2002).

Another important limitation to this study is that we did not explicitly account for particle coagulation or growth by condensation in our methodology for estimating emission rates. Coagulation has been shown to be a factor in indoor environments primarily during the first few minutes of high concentration periods (e.g., >20,000 cm^{-3}) for particles smaller than 20 nm, and particularly for those smaller than 10 nm (Wallace et al., 2008; Rim et al., 2012). Fig. 2 shows that there may have been some additional losses from the smallest size bin due to coagulation and/or condensation growth, as peak concentrations lagged other sizes by 3–5 min. However, it is not clear whether this is due to particle growth or mixing issues or, alternatively, that the difference is meaningful. Because we could not conduct controlled experiments in the test space with limited access, this potential evolution is difficult to evaluate precisely and is not explicitly accounted for herein, which may introduce some additional uncertainty in our estimates of size-resolved emission rates. However, emission rates of total UFPs based on the lumped loss rate approach are not affected by coagulation or condensation growth, as these mechanisms only impact individual bins within the total UFP range and no emissions were observed for particles greater than the 116 nm size bin. Regardless, particle growth and/or coagulation should be explored in more controlled environments in future studies.

5. Conclusions

In this work, we present some of the first known measurements of which we are aware of UFP emissions from commercially available desktop 3D printers. Emission rates of total UFPs were approximately an order of magnitude higher for 3D printers utilizing an ABS thermoplastic feedstock relative to a PLA feedstock: $\sim 1.9 \times 10^{11}$ # min^{-1} compared to $\sim 2.0 \times 10^{10}$ # min^{-1}. However,

both can be characterized as "high emitters" of UFPs. These results suggests caution should be used when operating some commercially available 3D printers in unvented or inadequately filtered indoor environments. Additionally, more controlled experiments should be conducted to more fundamentally evaluate aerosol emissions from a wider range of desktop 3D printers and feedstocks.

Acknowledgments

The authors thank Robert Zylstra and Julie Friedman Steele from The Metaspace and The 3D Printer Experience, respectively, for providing access to the test space.

References

Afshari, A., Matson, U., Ekberg, L.E., 2005. Characterization of indoor sources of fine and ultrafine particles: a study conducted in a full-scale chamber. Indoor Air 15, 141–150.

Andersen, Z.J., Olsen, T.S., Andersen, K.K., Loft, S., Ketzel, M., Raaschou-Nielsen, O., 2010. Association between short-term exposure to ultrafine particles and hospital admissions for stroke in Copenhagen, Denmark. European Heart Journal 31, 2034–2040.

Anderson, J.M., Shive, M.S., 1997. Biodegradation and biocompatibility of PLA and PLGA microspheres. Advanced Drug Delivery Reviews 28, 5–24.

Baughman, A.V., Gadgil, A.J., Nazaroff, W.W., 1994. Mixing of a point source pollutant by natural convection flow within a room. Indoor Air 4, 114–122.

Bumgarner, B., 2013. Getting started with a 3D printer. Make, 12–16.

Buonanno, G., Morawska, L., Stabile, L., 2009. Particle emission factors during cooking activities. Atmospheric Environment 43, 3235–3242.

Chalupa, D.C., Morrow, P.E., Oberdörster, G., Utell, M.J., Frampton, M.W., 2004. Ultrafine particle deposition in subjects with asthma. Environmental Health Perspectives 112, 879–882.

Contos, D.A., Holdren, M.W., Smith, D.L., Brooke, R.C., Rhodes, V.L., Rainey, M.L., 1995. Sampling and analysis of volatile organic compounds evolved during thermal processing of acrylonitrile butadiene styrene composite resins. Journal of the Air & Waste Management Association 45, 686–694.

Delfino, R.J., Sioutas, C., Malik, S., 2005. Potential role of ultrafine particles in associations between airborne particle mass and cardiovascular health. Environmental Health Perspectives 113, 934–946.

Dennekamp, M., 2001. Ultrafine particles and nitrogen oxides generated by gas and electric cooking. Occupational and Environmental Medicine 58, 511–516.

Hans, M.., Lowman, A., 2002. Biodegradable nanoparticles for drug delivery and targeting. Current Opinion in Solid State and Materials Science 6, 319–327.

He, C., Morawska, L., Taplin, L., 2007. Particle emission characteristics of office printers. Environmental Science & Technology 41, 6039–6045.

He, C., Morawska, L., Wang, H., Jayaratne, R., McGarry, P., Richard Johnson, G., Bostrom, T., Gonthier, J., Authemayou, S., Ayoko, G., 2010. Quantification of the relationship between fuser roller temperature and laser printer emissions. Journal of Aerosol Science 41, 523–530.

Hinds, W.C., 1999. Aerosol Technology: Properties, Behavior, and Measurement of Airborne Particles. Wiley-Interscience.

Johnston, C., Finkelstein, J.N., Mercer, P., Corson, N., Gelein, R., Oberdörster, G., 2000. Pulmonary effects induced by ultrafine PTFE particles. Toxicology and Applied Pharmacology 168, 208–215.

Klepeis, N.E., 1999. Validity of the uniform mixing assumption: determining human exposure to environmental tobacco smoke. Environmental Health Perspectives 107 (Suppl. 2), 357–363.

Von Klot, S., Wölke, G., Tuch, T., Heinrich, J., Dockery, D.W., Schwartz, J., Kreyling, W.G., Wichmann, H.E., Peters, A., 2002. Increased asthma medication use in association with ambient fine and ultrafine particles. European Respiratory Journal 20, 691–702.

Morawska, L., He, C., Johnson, G., Jayaratne, R., Salthammer, T., Wang, H., Uhde, E., Bostrom, T., Modini, R., Ayoko, G., McGarry, P., Wensing, M., 2009. An investigation into the characteristics and formation mechanisms of particles originating from the operation of laser printers. Environmental Science & Technology 43, 1015–1022.

Oberdörster, G., Celein, R.M., Ferin, J., Weiss, B., 1995. Association of particulate air pollution and acute mortality: involvement of ultrafine particles? Inhalation Toxicology 7, 111–124.

Oberdörster, G., Oberdörster, E., Oberdörster, J., 2005. Nanotoxicology: an emerging discipline evolving from studies of ultrafine particles. Environmental Health Perspectives 113, 823–839.

Oberdörster, G., Sharp, Z., Atudorei, V., Elder, A., Gelein, R., Kreyling, W., Cox, C., 2004. Translocation of inhaled ultrafine particles to the brain. Inhalation Toxicology 16, 437–445.

Penttinen, P., Timonen, K.L., Tiittanen, P., Mirme, A., Ruuskanen, J., Pekkanen, J., 2001. Ultrafine particles in urban air and respiratory health among adult asthmatics. European Respiratory Journal 17, 428–435.

Peters, A., Wichmann, H.E., Tuch, T., Heinrich, J., Heyder, J., 1997. Respiratory effects are associated with the number of ultrafine particles. American Journal of Respiratory and Critical Care Medicine 155, 1376–1383.

Ragan, S., 2013. Plastics for 3D printing. Make, 22.

Rim, D., Green, M., Wallace, L., Persily, A., Choi, J., 2012. Evolution of ultrafine particle size distributions following indoor episodic releases: relative importance of coagulation, deposition and ventilation. Aerosol Science and Technology 46, 494–503.

Rutkowski, J.V., Levin, B.C., 1986. Acrylonitrile-butadiene-styrene copolymers (ABS): pyrolysis and combustion products and their toxicity–a review of the literature. Fire and Materials 10, 93–105.

Schaper, M.M., Thompson, R.D., Detwiler-Okabayashi, K.A., 1994. Respiratory responses of mice exposed to thermal decomposition products from polymers heated at and above workplace processing temperatures. American Industrial Hygiene Association Journal 55, 924–934.

Sioutas, C., Delfino, R.J., Singh, M., 2005. Exposure assessment for atmospheric ultrafine particles (ufps) and implications in epidemiologic research. Environmental Health Perspectives 113, 947–955.

Stölzel, M., Breitner, S., Cyrys, J., Pitz, M., Wölke, G., Kreyling, W., Heinrich, J., Wichmann, H.-E., Peters, A., 2007. Daily mortality and particulate matter in different size classes in Erfurt, Germany. Journal of Exposure Science & Environmental Epidemiology 17, 458–467.

Unwin, J., Coldwell, M.R., Keen, C., McAlinden, J.J., 2012. Airborne emissions of carcinogens and respiratory sensitizers during thermal processing of plastics. Annals of Occupational Hygiene 57, 399–406.

Wallace, L., Wang, F., Howard-Reed, C., Persily, A., 2008. Contribution of gas and electric stoves to residential ultrafine particle concentrations between 2 and 64 nm: size distributions and emission and coagulation rates. Environmental Science & Technology 42, 8641–8647.

Wallace, L.A., Emmerich, S.J., Howard-Reed, C., 2004. Source strengths of ultrafine and fine particles due to cooking with a gas stove. Environmental Science & Technology 38, 2304–2311.

Weinhoffer, E., 2012. 3D printing FAQ. Make. http://makezine.com/magazine/make-ultimate-guide-to-3d-printing/3d-printing-faqs/, (accessed 12.07.13.).

Zitting, A., Savolainen, H., 1980. Effects of single and repeated exposures to thermo-oxidative degradation products of poly(acrylonitrile-butadiene-styrene) (ABS) on rat lung, liver, kidney, and brain. Archives of Toxicology 46, 295–304.